Supporting Information for Water Content of Greenland Ice Estimated from Ground Radar and Borehole Measurements

S1 Borehole information

Three boreholes separated by <30 m were drilled in 2011 at S3, and four holes separated by <50 m were drilled in 2012 at GL12-S2 (Table S1). Sensor strings with various instruments including thermistors spaced on 20 m intervals were deployed into the boreholes and allowed to freeze into the ice and equilibrate with the ambient ice temperature. Temperature data were retrieved from each location in September following the instrumentation as well as the following summer. For more information about the methods and interpretation of the temperature data see Harrington et al. (2015).

S2 Ray inversion on migrated vs unmigrated data

As we state in the main body of the text, we used unmigrated data (in conjunction with borehole depth and temperature measurements at S3 and S4) to construct the initial velocity model for the ray based traveltime inversion. The common offset GPR profiles (Figs. 2 & 3, main text) reveal a large (~18º) bed dip angle between ~200 m and 650 m distance from S3. Because the data is unmigrated, the apparent dip in this region is less than the true dip angle. To determine if the inversion is sensitive to the difference in the apparent dip based on migrated vs. unmigrated data we migrated the 2.5 MHz data using a 2D Kirchhoff depth migration algorithm in SeisUNIX (sukdmig2d). The data were migrated with a homogeneous velocity model with the velocity assumed to be equal to the average GPR propagation speed measured at S3 (1.61×10^8 m s^{-1}). Figure S1, below, show the result of the migration as well as the original data. We picked the bed reflection in both the migrated as well as the unmigrated data and compared the results (Fig. S2). It is apparent from the migrated data that the simple velocity model under-migrates the point-source reflections in the upper ~200 m of the profile (the hyperbolas from the point source reflector at ~200 m distance, 75-125 m depth are not fully collapsed) and over-migrates the data near the bed (reverse hyperbolas emanating from the bed slope change at ~200 m distance and ~475 m depth). The picks made on both data reveal that there is negligible difference in the bed geometry of the migrated and unmigrated data between 0 and 200 m distance as well as between 650 and 840 m distance.

Since the ray tracing inversion used in this study does not have bed reflections beyond 120 m distance, the results for the ray tracing inversion are valid for initial velocity models based on both migrated as well as unmigrated data.

S3 Where the water is being held within the ice

While the cold layer may not have grain-scale water our common offset imaging of englacial hyperbolas imply macro-scale water bodies are present in this layer. Point reflectors in similar data have been interpreted either as near surface crevasses (presumably the same as water filled voids) or surface crevasses that are off-axis from the radar profile (Catania et al., 2008). The hyperbolic diffractions in our common offset data are unlikely to result from a distant near-surface source, since the theoretical and measured radiation pattern of a dipole antenna (Arcone, 1995) greatly limits this possibility: the relative signal strength of off nadir, near surface reflections would be weak compared to reflections generated at nadir, and we do not observe that. Rather, the diffractions observed in our profiles are strong, indicating that they likely arise from near-nadir discontinuities. Similar hyperbolic returns in the cold ice layer of polythermal glaciers have been observed prior to any seasonal melt, and have been interpreted as meter scale water bodies persisting through the winter (e.g.; Pälli et al., 2002). Therefore, our working hypothesis is that the cold layer contains sparse large water inclusions up to several hundred meters below the surface, perhaps generated in a crevassed area about 3 km up flow from the site. Further, since our estimates of liquid water content are derived under the assumption of negligible water content in the upper layer, our wetness values for the temperate layer would be slightly high if the englacial bodies that produce the point reflections seen in the common offset radar data contain non-negligible volumes of liquid water.

S4 Error estimates

S4.1 Error in borehole depth measurements

The borehole depth measurements are derived from the measured length of hot water drill hose that is in the hole when the bed is reached during drilling. There is certainly some amount of strain in the hose that we cannot accurately account for. We assign an error in the depth of the boreholes at each location that is equal to the variation in borehole depths at that location; at S3 the variation is 9 m, at S4 the variation is 22 m. Errors in depth associated with variations of the boreholes from vertical (plumb) are negligible.

S4.2 Error in picking TWT to reflection horizons

As we state in the main manuscript, we determined the TWT to the bed at each borehole location from the 10 MHz GPR data. This data is recorded on a time interval of 8×10^{-9} s. We conservatively estimate the error in the TWT at each borehole location by picking the top and bottom of each high amplitude reflection event that corresponds to the bed reflection. At S3 this corresponds to 184×10^{-9} s (or 23 times the sampling rate), at S4 this corresponds to 88×10^{-9} s (or 11 times the sampling rate). Conventionally, the accuracy of GPR is considered to be ~1/4 wavelength of the signal. In the 5 MHz data, ¼ wavelength is approximately 32×10^{-9} s. We believe that the variation of both the ice thickness and surface elevation along our profile require that we use the much more conservative error estimates stated above.

Because the relationship between TWT and GPR propagation speed is linear, the errors approximated for the TWT propagate directly to error associated with velocity.

S4.3 Error in linear fit to the direct interfacial surface wave in the single moveout multi-offset data

The error estimate of the linear fit to the direct interfacial surface wave in the single moveout multi-offset data was derived from directly varying the assumed GPR propagation velocity to fit the surface wave data. We found that the velocity range that fit the data was 1.68 x 10^8 m s^{-1} to 1.70 x 10^8 m s^{-1}, or 1.69 x 10^8 m s^{-1} ± 0.01 x 10^8 m s^{-1}.

S4.4 Error in wetness calculation

To determine the error associated with the average wetness values calculated with a direct comparison of TWT to depth conversion for the bed reflection we calculated the range in wetness values associated with the error in TWT picks of the bed at both S3 and S4.

S4.5 Error in ray based traveltime inversion

We do not attempt to estimate the error for our two-layer velocity models since inverting for the velocity profile of a two-layer system is non-unique and the constraints on the inversion are not sufficient to accurately estimate the error. Instead, we fit the data to a reasonable RMS traveltime residual.

S4.6 Method and error estimation in two-layer direct comparison of TWT and borehole depth

The two-layer TWT to depth calculation for temperate layer thickness assumes no error in the velocity within the cold layer. The depth of the temperate layer at S3 and S4 is accurate to 20 m, which is the spacing of the thermistors in the borehole. We therefore calculate the GPR propagation velocity using a temperate layer thickness halfway between the uppermost thermistor at the pressure melting point and the next higher thermistor. We calculate the GPR propagation velocity within the temperate layer with Eq. (S1)

$$v_{temperate} = \frac{(v_{average} * h_{total}) - (v_{cold} * h_{cold})}{h_{temperate}} \quad \text{(S1)}$$

Where h is thickness and v is the GPR propagation speed. To estimate the error in our calculations, we solve for the extreme values: (1) large temperate layer with low velocity, and (2) smaller temperate layer with high velocity. The resultant range of temperate layer velocity are used to calculate the wetness with the CRIM and Looyenga (1965) 2-phase mixing model equations. We conservatively estimate the error as the largest variation from the initial estimate of the temperate layer wetness.

References

Arcone, S. A.: Numerical studies of the radiation patterns of resistively loaded dipoles, J. Appl. Geophys., 33(1-3), 39–52, doi:10.1016/0926-9851(95)90028-4, 1995.

Catania, G. A., Neumann, T. A. and Price, S. F.: Characterizing englacial drainage in the ablation zone of the Greenland ice sheet, J. Glaciol., 54(187), 567–578, doi:10.3189/002214308786570854, 2008.

Harrington, J. A., Humphrey, N. F. and Harper, J. T.: Temperature distribution and thermal anomalies along a flowline of the Greenland ice sheet, Ann. Glaciol., 56(70), 98–104, doi:10.3189/2015AoG70A945, 2015.

Looyenga, H.: Dielectric constants of heterogeneous mixtures, J. Glaciol., 31(3), 401–406, 1965.

Pälli, A., Kohler, J. C., Isaksson, E., Moore, J. C., Pinglot, J. F., Pohjola, V. A. and Samuelsson, H.: Spatial and temporal variability of snow accumulation using ground-penetrating radar and ice cores on a Svalbard glacier, J. Glaciol., 48(162), 417–424, doi:10.3189/172756502781831205, 2002.

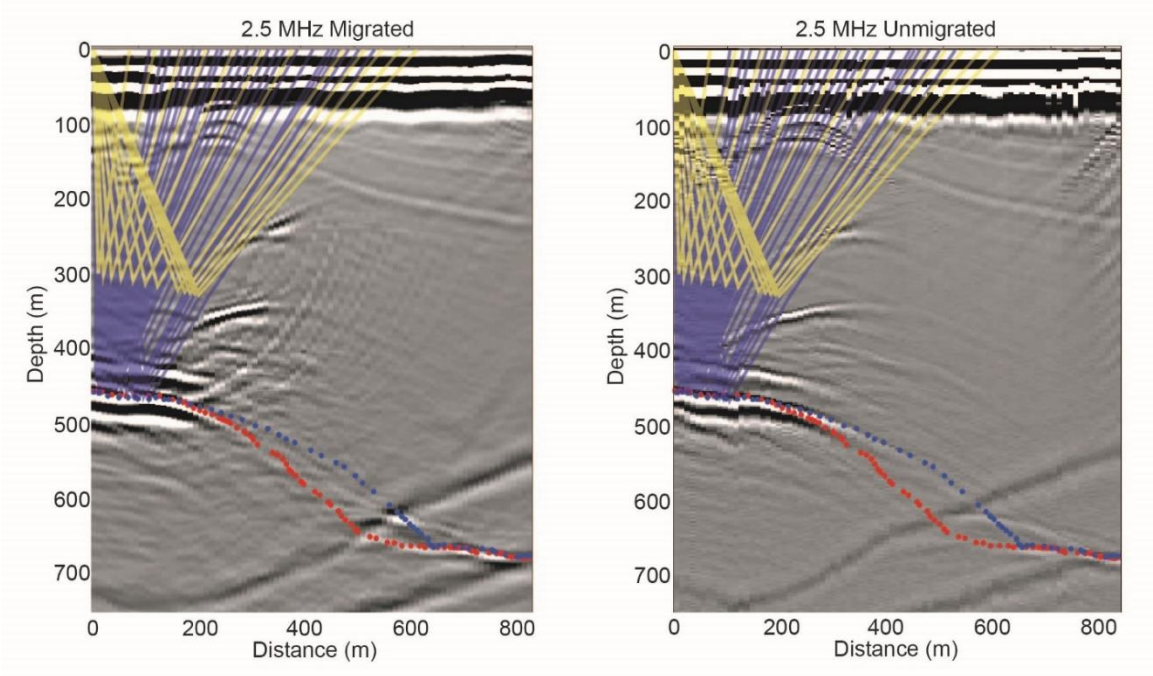

Figure S1. Migrated (left) and unmigrated (right) images from 2.5 MHz GPR transect. Bed picks are shown on both images, blue dots are picks of the migrated bed, red dots are picks of the unmigrated bed. Rays used in traveltime inversion are shown to highlight that rays are not traced in the region where the migration increases the bed slope. Note that, unlike Fig. 2 in the main manuscript, the rays in both images appear to cross the bed reflection; this is due to the simple velocity model used to migrate the data and convert from TWT to depth.

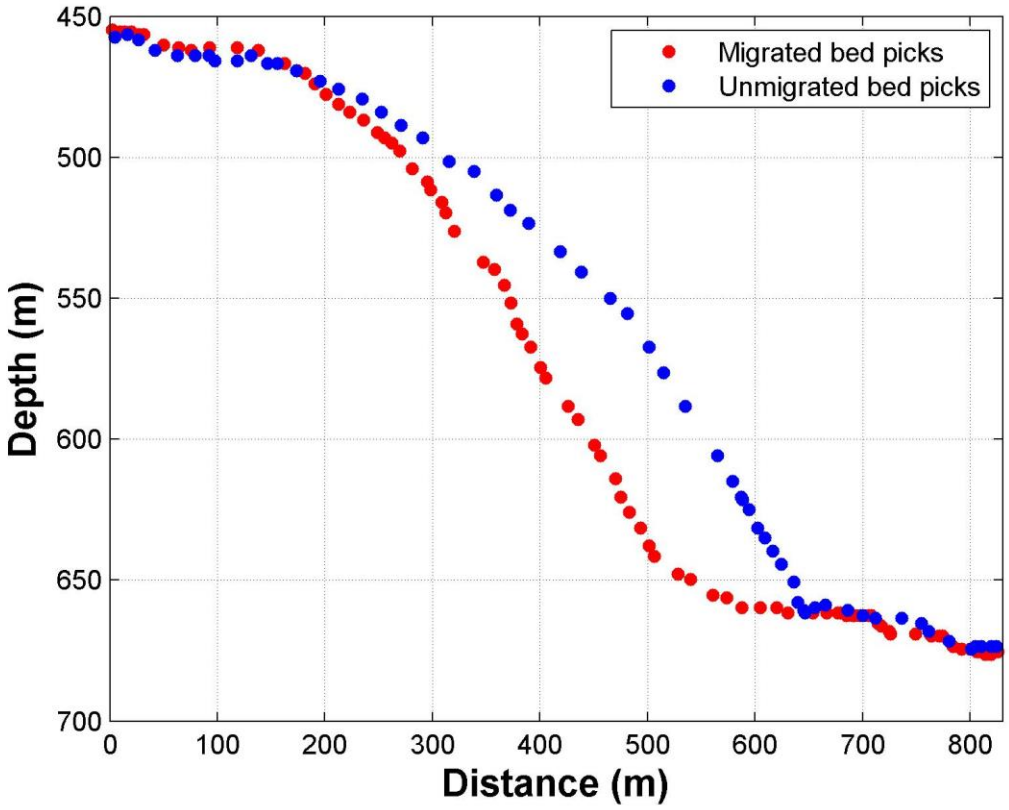

Figure S2. Bed reflection picks from 2.5 MHz common offset GPR data showing consistent depth in both data in the region that affects the traveltime ray inversion algorithm.

Borehole	Latitude	Longitude	Elevation	Date	Depth	Temperature profile
S3	67.19517	-49.7192	849 m	July 2, 2011	457 m	Y
				July 4, 2011	466 m	Y
				July 6, 2011	459 m	Y
S4	67.02396	-49.7179	822 m	June 13, 2012	695 m	Y
				June 15, 2012	710 m	N
				June 17, 2012	688 m	Y
				June 20, 2012	696 m	Y

Table S1. Location, depth, and date drilled for the boreholes at S3 and S4.